Puzzle of the Intramolecular Hydrogen Bond of Dibenzoylmethane Resolved by Molecular Dynamics Simulations

Etinski, M.; Ensing, B.

DOI
10.1021/acs.jpca.8b01930

Publication date
2018

Document Version
Final published version

Published in
The Journal of Physical Chemistry. A

THE JOURNAL OF PHYSICAL CHEMISTRY A

Article

Cite This: J. Phys. Chem. A 2018, 122, 5945−5954

pubs.acs.org/JPCA

Puzzle of the Intramolecular Hydrogen Bond of Dibenzoylmethane Resolved by Molecular Dynamics Simulations

Mihajlo Etinski*,† and Bernd Ensing*,‡

†Faculty of Physical Chemistry, University of Belgrade Studentski trg 12-16 11000 Belgrade, Serbia

‡Van 't Hoff Institute for Molecular Sciences (HIMS), University of Amsterdam, Science Park 904, 1098 XH Amsterdam, The Netherlands

ABSTRACT: The enol form of dibenzoylmethane has been the subject of many experimental and theoretical studies, yet the symmetry and the spectral response of the OHO intramolecular hydrogen bond remains mysterious due to conflicting assignments. In order to qualitatively understand the complex proton dynamics, it is necessary to probe the neighborhood of stationary points on the potential energy landscape. Here, we employ density functional theory-based molecular dynamics (DFT-MD) simulations to sample the coupling between the intermolecular proton transfer and all other molecular modes. To account for the quantum nature of the proton motion, we employ the path integral formalism within the DFT-MD simulations. Our results reveal that the hydrogen-bonded proton is delocalized between two oxygen atoms with sightly higher probability to be observed in the asymmetric than the symmetric position. The simulated infrared spectrum is found to be in a reasonably good agreement with the experimental spectrum. The computed ν_{OH} band is remarkably broad and centered around 2640 cm^{-1}. The origin of the discrepancy between the simulated and experimental intensities of the ν_{OH} band is discussed.

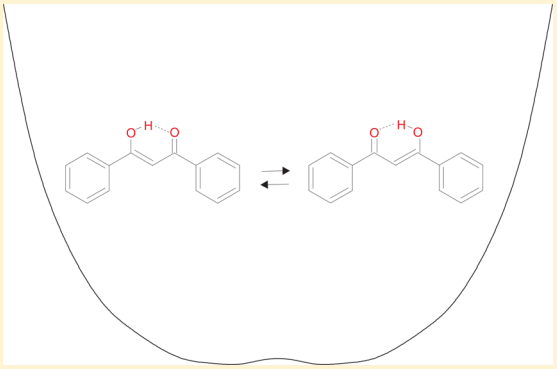

INTRODUCTION

Hydrogen bonds control the structure and function of a vast range of protic molecules and their assemblies. A hydrogen bond is an attractive interaction between an electronegative acceptor atom A and a positively charged hydrogen atom that is covalently attached to an electronegative donor atom D. Hydrogen bond energies range from 1 until 40 kcal/mol, which is more than that of van der Waals interactions and less than covalent or ionic bonds.[1] The donor and acceptor atoms might belong to the same or to two different molecules, thus forming an *intra*-molecular or an *inter*-molecular hydrogen bond, respectively. The adiabatic potential for the proton transfer between the donor and acceptor atoms varies from a double-well potential, associated with the asymmetric D−H···A and D···H−A structures at relatively large donor−acceptor distances, to a single-well for a symmetric D···H···A hydrogen bond at short D−A distances.[2,3] In the former case, the proton is localized on the donor or the acceptor atom, while in the latter case it is delocalized between these atoms.

In most cases, the symmetry of the hydrogen bond can be determined accurately with neutron diffraction spectroscopy. However, if the two minima on the potential energy surface are very close and the barrier for proton transfer is low, resolving the structure is difficult due to fast proton exchange between the minima. In such cases, complementary techniques, such as NMR spectroscopy and computational studies are needed to provide insight into the hydrogen bonding properties.

The enolic forms of β-diketone compounds exhibit strong O−H···O intramolecular hydrogen bonds at rather short donor−acceptor O···O distances.[4] The longest O···O distance is found in malonaldehyde (2.55 Å[5]), which is the simplest member of the β-diketone family. By adding substituents to malonaldehyde, this distance can decrease to 2.54 (acetylacetone[6,7]), 2.50 (benzoylacetone[8]), or even 2.45−2.46 Å (dibenzoylmethane[9−13]). Malonaldehyde has an asymmetric hydrogen bond.[5,14−26] The potential energy barrier for the proton transfer has been computed to be 4.09 kcal/mol at CCSD(T)/aug-cc-pV5Z level.[19] In the case of acetylacetone, most studies have argued that the bridging hydrogen bond is asymmetric,[6,7,27−35] although several studies reached the opposite conclusion.[36−38] Even less consensus exists with regard to the symmetry of the H-bond in dibenzoylmethane (DBM), a molecule which is employed as a UVA filter in cosmetic sunscreens.[39−41] Early X-ray diffraction studies[9,10] found similar, although not identical, geometric parameters for the asymmetric hydrogen bond of DBM. Gilli et al. combined a statistical analysis of X-ray data with quantum chemical calculations and proposed that the potential energy surface for the proton transfer between the oxygen atoms is a weakly asymmetric single-well profile.[4] Electronic density images from

Received: February 25, 2018
Revised: June 29, 2018
Published: June 29, 2018

DOI: 10.1021/acs.jpca.8b01930
J. Phys. Chem. A 2018, 122, 5945−5954

a more recent X-ray measurement performed by Thomas et al.[13] show a migration of the bonding density from an asymmetric position at low temperatures to an almost centered position at room temperature. However, gas phase electron diffraction experiments reported a strongly asymmetric structure.[42] In addition, room-temperature neutron diffraction experiments suggested an asymmetric structure invariant with temperature.[13,43] Borisov et al.[44] performed an NMR study and found that, in the temperature range from 181 to 268 K, a tautomeric equilibrium exists between the two asymmetric enolic structures (see Figure 1). Furthermore, Masuda et al.[45]

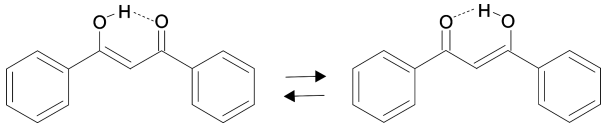

Figure 1. Tautomeric equilibrium between the two asymmetric enolic structures of dibenzoylmethane (DBM).

reported an NMR study at room-temperature of DBM in CCl_4, in which they proposed a nearly symmetric hydrogen bond with the potential energy profile for the proton transfer being either a single-well or a double-well with a barrier below the zero-point energy. In polar solvents such as DMSO and MeOH, the proton tends to localize at one oxygen atom due to solute−solvent interactions.[46] More recently, Kong et al. addressed the DBM's hydrogen bond properties in solid state by NMR and classical ab initio molecular dynamics[47] and found that the potential energy barrier for the proton transfer is below the ground state vibrational level. Feyer et al. measured the core level photoemission spectrum of gaseous DBM and provided evidence that the point group symmetry of the ground state is C_{2v}.[38]

The hydrogen bond dynamics can be also probed by infrared spectroscopy. Because of the strong intramolecular hydrogen bond in DBM, it is expected that the stretching mode of the hydroxyl group, ν_{OH}, is significantly red-shifted and broadened due to the complex proton dynamics, which includes proton transfer and energy redistribution to other modes. The infrared spectrum is characterized by a strong band around 1600 cm^{-1} and an extremely broad and weak band from 2200 to 3500 cm^{-1}.[48−52] The latter band has a maximum around 2700 cm^{-1} in carbon tetrachloride solution. In a 1949 article, Rasmussen et al. attributed this band to the ν_{OH} mode.[48] This assignment was later confirmed by Bratož et al.[49] In addition, the in-plane, δ_{OH}, and out-of-plane, γ_{OH}, O−H bending modes were related by these authors to peaks at 1470 and 960 cm^{-1}, respectively, whereas the C−O stretching bands were assigned to 1605 and 1302 cm^{-1} in carbon tetrachloride solution. Recently, a new assignment of the O−H stretching mode was tentatively proposed by Hansen et al.[52] They argued that since the O···O distance in DBM is 0.08 Å shorter than in acetylacetone, its O−H stretching peak should be located at much smaller wavenumbers than that in the case of acetylacetone (≈ 2800 cm^{-1}).[34,50] On the basis of quantum chemical calculations, Hansen et al. proposed that the O−H stretching frequency is close to 1550 cm^{-1} and responsible for the strong band seen at that wavenumber.[52] This conclusion is in line with a significant enhancement of the intensity, ν_{OH}, due to the electric anharmonicity for hydrogen bonds whose donor−acceptor distances are in the range of 2.4−2.5 Å, as predicted by Athokpama et al.[53]

Petković and Etinski examined the structure of an isolated DBM molecule and its ν_{OH} frequency using quantum chemical methods and dimensionally reduced models of the potential energy surface.[54] The potential energy barrier for the proton transfer was computed to be in the range from 0.8 to 2.0 kcal/mol depending on the employed electronic structure method and basis set. On the basis of these values, these authors proposed that both asymmetric and symmetric structures of DBM are present in the gas phase. Furthermore, they estimated the O−H (for asymmetric structure) and O···H···O (for symmetric structure) stretching frequencies to be ≈2400 and 500 cm^{-1}, respectively.

In this contribution, we employ classical and path integral ab initio Born−Oppenheimer molecular dynamics to address the structure of DBM's hydrogen bond and its infrared spectrum in the gas phase. This method allows us to go beyond selected degrees of freedom and to consider all molecular degrees of freedom and their couplings. Sampled trajectories capture information about the mechanical and electrical anharmonicity as well as thermal fluctuations, and thus provide an accurate measure of the hydrogen bond symmetry and the line shape of the infrared spectrum at room temperature. Although the quantum effects are important for strong hydrogen bonds,[3] we will show that even classical mechanics can reasonably well simulate the properties of the intramolecular hydrogen bond of DBM.

The paper is organized as follows. In the next section, we summarize the computational methods that were employed in our calculations. In the subsequent section, we discuss the minimum energy structure and present a one-dimensional model for the proton transfer. Furthermore, the consequences of quantum effects and thermal fluctuations on the geometry of DBM are presented and discussed. In the following subsection, a simulated infrared spectrum is assigned and discussed. Finally, we draw conclusions from our study.

■ COMPUTATIONAL DETAILS

All calculations were performed with the CP2K program package.[55] We utilized the BLYP functional[56,57] based on the generalized gradient approximation and Grimme's D3 correction for dispersion interaction.[58] The electron density was expanded using a mixed Gaussian and plane waves (GPW) method[59] with a DZVP basis set for the localized functions. The finest grid level cutoff and relative cutoff were set to 350 and 50 Ry, respectively. A pseudopotential of the GTH type[60] was used to represent core electrons. The simulation was performed in a cubic box with a box size of 15 Å under nonperiodic conditions. The wavelet method[61,62] was used for proper treatment of the isolated system. The SCF convergence was set to 5.0×10^{-7} in atomic units. The nuclei were propagated with a time step of 0.5 fs. The CSVR thermostat[63] was employed in order to simulate a canonical ensemble at 300 K. Nuclear quantum effects were taken into account using the path integral approach implemented in the CP2K program. The number of replicas to describe the atomic nuclei was taken to be 16. The classical (quantum) simulations were carried out for 30 and 8 ps after thermal equilibration runs of 10 and 2 ps. The infrared spectrum was calculated from classical dynamics trajectories using the following protocol. A total of 15 configurations from the equilibriated *NVT* trajectory were selected at 2 ps intervals. These configurations were further propagated in the microcanonical ensemble for 20 ps. Maximally localized Wannier orbitals were computed along

DOI: 10.1021/acs.jpca.8b01930
J. Phys. Chem. A 2018, 122, 5945−5954

each of the NVE trajectories to calculate the dipole moment and its time autocorrelation function. The average over the whole set of the trajectories yielded the infrared and power spectra. Both spectra were computed using the TRAVIS software.[64,65]

RESULTS AND DISCUSSION

Optimized Geometry. First, we assess the ability of the BLYP functional, augmented with the D3 dispersion correction, to model the structure of the DBM molecule. The bond lengths of the optimized geometry of DBM at the BLYP+D3/GPW, and the M06-2X/cc-pVTZ[54] levels of theory are shown in Figure 2, together with data from neutron

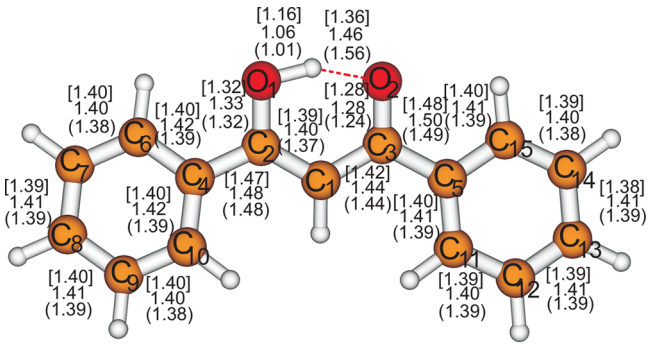

Figure 2. Bond lengths within the optimized DBM geometry at the BLYP+D3/GPW and M06-2X/cc-pVTZ[54] (in brackets) levels of theory, compared to neutron diffraction data at room temperature[43] (in square brackets).

diffraction experiments.[43] Note that the experimental data are obtained for a DBM crystal at room temperature. The optimized minimum on the potential energy surface corresponds to the asymmetric hydrogen bond, in which the proton is closer to one of the two oxygen atoms. Both functionals provide nonplanar equilibrium geometries, although the optimized structure with the M06-2X functional is more distorted. The C1−C3−C5−C11 and C1−C2−C4−C10 dihedral angles are −6 and −9 deg at the BLYP+D3 level and −17 and −19 deg at the M06-2X level. Generally, the M06-2X functional gives shorter bond lengths than the BLYP functional. Comparing the bond lengths within the benzene rings, we see very good agreement between the two functionals, with discrepancies of approximately 0.02 Å. Also the C1−C3 and C2−O1 bonds have very similar bond lengths. The main difference in the molecular structures obtained with the BLYP+D3 and M06-2X functionals comes from the description of an intramolecular hydrogen bond. Its length differs by 0.1 Å. The O1−H and O2−C3 bonds are also influenced by the hydrogen bond and their lengths differ by approximately 0.05 Å. The O···O distance is 2.46 Å with BLYP+D3/GPW and 2.49 Å with M06-2X/cc-pVTZ. Overall, we conclude that the BLYP density functional, corrected with the dispersion term, provides similar structural parameters as the more advanced M06-2X functional. Surprisingly, the BLYP+D3/GPW optimized geometry agrees even better with the neutron diffraction data[43] than the M06-2X/cc-pVTZ result. On average, the BLYP+D3 bond lengths are within 0.01 Å of the experimentally obtained geometry. The exceptions are the O1−H and O2···H bonds, which differ by 0.1 Å. In the next sections, we will argue that quantum effects and anharmonicity of the potential minimum can considerably modify the hydrogen bond length.

The proton transfer potential energy barrier determines the vibrational response of the β-diketons' OHO moiety.[34,51] We find that the barrier height is more sensitive to the computational level than the molecular geometry parameters. The barrier is 0.7 kcal/mol at the BLYP+D3/GPW level. The M06-2X/cc-pVTZ and ab initio correlated levels of theory MP2/cc-pVDZ and CC2/cc-pVTZ give barriers which are 1.1, 1.3, and 0.1 kcal/mol[54] higher than the BLYP+D3 value, respectively. Hence, the BLYP+D3 functional underestimates the barrier height comparing to the M06-2X functional and MP2 method but gives a similar value as the CC2 method. In the absence of the CCSD(T) value in the basis set limit it is difficult to estimate the correct barrier value. The comparison of the simulated and the experimental infrared spectrum might provide additional insight into the plausibility of the BLYP+D3/GPW barrier value. Meuwly and co-workers demonstrated the correlation between the center frequency of the O−H stretching band and the proton transfer barrier.[34,66] These authors developed a method to modify force-field parameters responsible for the proton transfer potential in such a way that the overall shape of the potential energy surface remained topologically similar but differed in the proton transfer barrier value. By employing this potential energy morphing, they simulated several O−H stretching bands of acetylacetone with different barrier values.[34] A direct comparison with experiment enabled them to qualitatively determine the proton transfer barrier of acetylacetone. Thus, this method provides an indirect way to extract the proton transfer barrier in cases when the size of the system does not allow the CCSD(T) calculations.

One-Dimensional Model of the Proton Transfer. The optimized geometry provides only limited information on the hydrogen bond, since the atoms are in constant motion due to quantum effects and thermal fluctuations. The potential barrier for the proton transfer is found to be very low and it is not certain whether the ground state vibrational level is below or above the barrier. To address this issue, we consider here a one-dimensional quantum mechanical model of the proton transfer. Although this reduced model represents a simplified picture of the proton transfer, it provides some interesting physics insights. We focus on the asymmetric coordinate $\Delta(\mathrm{OH})$, which is composed of the difference between the two O−H distances. The potential energy along this coordinate was calculated using restrained optimizations. The force constant for the harmonic restraining potential was 1.0 au, which effectively constrains the coordinate. The one-dimensional Schrödinger equation was solved on this potential employing the Fourier grid Hamiltonian method.[67] The mass of the particle was chosen to be equal to the proton mass, assuming that the oxygen atoms are connected to the heavy fragments ($-\mathrm{C}-\mathrm{C_6H_5}$), so that the motion of the hydrogen atom can be separated from the other degrees of freedom.

The potential energy along the proton transfer coordinate and the resulting energy levels are shown in Figure 3. The barrier for the proton transfer is 240 $\mathrm{cm^{-1}}$. The ground state level lies 74 $\mathrm{cm^{-1}}$ below the barrier. Its wave function has a double maximum at $\Delta(\mathrm{OH}) = \pm 0.27$ Å, which can be related to the length of the O−H bond.[3] Note that tunneling through the barrier and anharmonicity shift the most probable value of the $\Delta(\mathrm{OH})$ coordinate by 0.12 Å from the value in the optimized structure. In addition, the ground state wave

DOI: 10.1021/acs.jpca.8b01930
J. Phys. Chem. A 2018, 122, 5945−5954

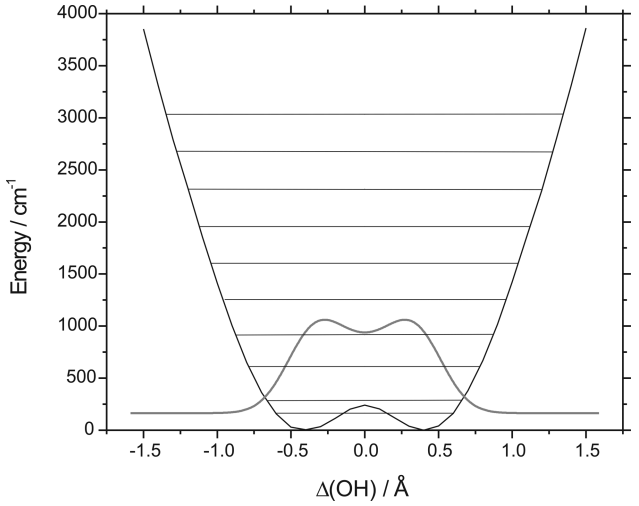

Figure 3. One-dimensional potential energy for the proton transfer coordinate Δ(OH) and its energy levels. The ground state wave function is depicted in gray.

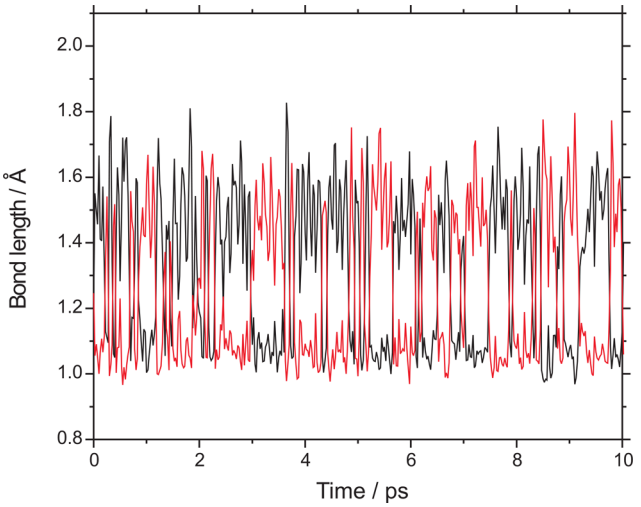

Figure 4. Instantaneous O−H distances in the first 10 ps of the simulation in which the atoms are treated classically: red line, O1−H bond; black line, O2−H bond.

function has substantial probability density in between the oxygen atoms. The first excited state lies 47 cm^{-1} above the barrier. It has a node in the center, and the maxima of its wave function are more displaced toward the oxygen atoms. The energies of the third, fourth and fifth states are 373, 674, and 1016 cm^{-1} above the barrier. The energy difference between the consecutive energy levels at higher energies is in the range from 300 to 350 cm^{-1}.

According to this model, the hydrogen bond is asymmetric with considerable probability for the proton to be found midway between the oxygen atoms. The second and third energy levels are accessible at room temperature and thus the hydrogen bond length will exhibit a small temperature dependence due to the different nodal structure of their wave functions. The energy difference between the ground state and the first excited state is 121 cm^{-1}. Therefore, the proton transfer between the oxygen atoms takes 275 fs, which might be very fast for certain experimental techniques aimed at resolving the proton position.

Thermal Effects on the Molecular Geometry. Although the one-dimensional model is a source of valuable information about the hydrogen bond, it does not account for coupling to other coordinates. Thus, in order to arrive at a more realistic picture of the hydrogen bond, which includes all coordinates and thermal effects, we performed molecular dynamics simulations in the canonical ensemble at 300 K using classical and path integral simulations.

Let us first discuss the results of the classical simulation. The classical dynamics lacks zero-point energy motion as well as the ability of tunneling through barriers. Because of thermal fluctuations, it probes the potential energy surface around its minimum. The potential barrier is low along the proton transfer coordinate and thermal fluctuations might induce vibrational-assisted thermal hopping. The instantaneous O−H distances are displayed in Figure 4. We clearly observe the proton hopping events approximately every 0.5 ps. Usually, four to five large amplitude oscillations are preceding the hopping event. These oscillations approximately correspond to frequency 250−350 cm^{-1}. Note that there are also small amplitude high-frequency oscillations which correspond to the proton oscillations around the local minima on the potential energy surface. The O−H distances are in the range from approximately 1.0 to 1.8 Å. Figure 5 shows the Helmholtz free

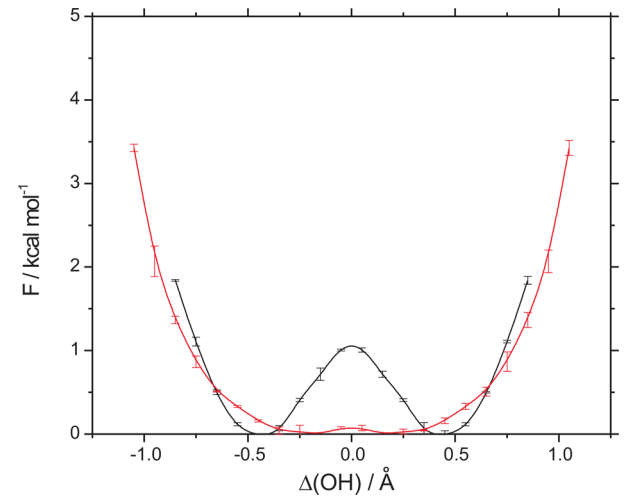

Figure 5. Helmholtz free energy for the proton transfer computed by the classical (black line) and quantum (red line) simulations. The free energy curves are symmetrized around the Δ(OH) = 0 value. The errors are estimated as a difference between the symmetrized and unsymmetrized curves.

energy profile as a function of the proton transfer Δ(OH) coordinate. It consists of the two minima at Δ(OH) ≈ ± 0.45 Å, separated by the barrier that amounts to ≈1.03 kcal/mol. Thus, the classical dynamics simulation finds the asymmetric hydrogen bond with the slightly elongated Δ(OH) coordinate due to thermal fluctuations. It is also noteworthy to examine the effect of thermal fluctuations to other coordinates. The probability distribution and averaged values of the selected geometry parameters are collected in Figure 6 and Table 1, respectively. The O1···O2 equilibrium distance increases by 0.03 Å due to thermal fluctuations. Its probability distribution takes values from 2.3 to 2.7 Å. At very small O1···O2 distances (<2.35 Å) the potential energy barrier for the proton transfer vanishes.[68] Therefore, the O1···O2 oscillations stimulate the proton transfer dynamics. The O1−H−O2 angle determines

DOI: 10.1021/acs.jpca.8b01930
J. Phys. Chem. A 2018, 122, 5945−5954

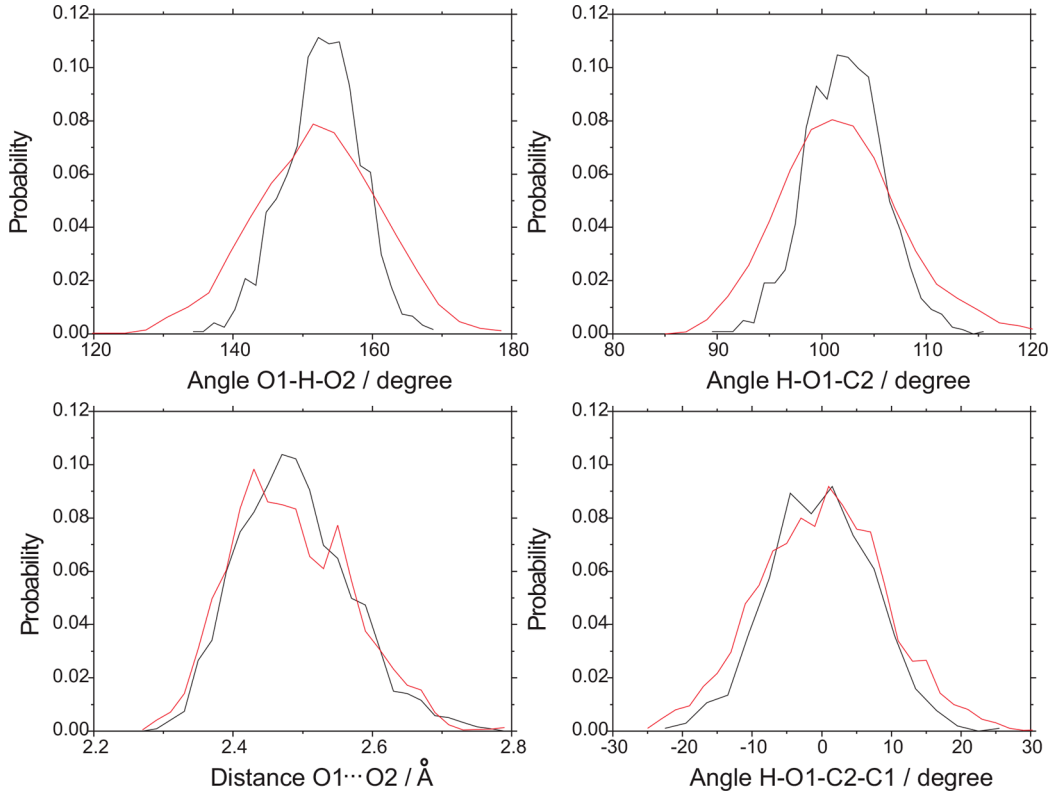

Figure 6. Probability distribution of the selected geometry parameters computed by classical (black line) and quantum (red line) simulations.

Table 1. Selected Averaged Geometry Parameters Computed by Classical and Quantum Simulations[a]

parameter	classical	quantum	opt. eq
O1···O2	2.49	2.48	2.46
O1−H−O2	153	152	155
H−O1−C2	102	102	104
H−O1−C2−C1	0	0	0

[a]Also, parameters from the optimized equilibrium structure are provided. Bond length is in Å; angles are in degrees.

the proton position relative to the oxygen atoms. Its optimized equilibrium value is 155 deg. In addition, thermal motion leads to a slight decrease of this angle to 153 deg. The same is valid for the H−O1−C2 angle, which represents the in-plane hydroxy group bending. On the other hand, the average value of the angle that determines the out-of-plane hydroxy group bending, remains unchanged by thermal fluctuations.

Having discussed the effects of thermal fluctuations on the molecular structure, let us proceed to the nuclear quantum effects on the geometry of DBM. As was shown in the one-dimensional model, the ground state for the motion along the proton transfer coordinate is 74 cm^{-1} below the barrier. Coupling of this motion to other degrees of freedom might shift this level above the barrier. Figure 5 shows the free energy profile along the proton transfer coordinate computed with the path integral molecular dynamics. The computed free energy exhibits a very shallow double-well profile indicating that the hydrogen bonded proton is delocalized between the oxygen atoms. The most probable value of the proton transfer coordinate corresponds to $\Delta(OH) = 0.15$ Å, which is 0.05 Å shorter than the value measured in a neutron diffraction experiment.[43] Thus, the thermal effects and coupling of the proton transfer coordinate to other degrees of freedom decrease even more the hydrogen bond length found in the one-dimensional proton transfer model. In addition, the free energy barrier separating two asymmetric configurations amounts to 0.07 kcal/mol. As was already discussed for the one-dimensional proton transfer model, the small free energy barrier easily enables thermal proton hopping between two asymmetric configurations. Note that Petković and Etinski[54] reported the free energy barrier of 0.59 kcal/mol, computed with the composite G4MP2 method, which includes scaled harmonic frequencies at B3LYP level and the electronic energy at Møller−Plesset perturbation and coupled cluster level. The ratio of the asymmetric and symmetric conformers in that case was 2.5, whereas in our case it is 1.1.

The probability distribution and averaged values of the selected geometry parameters computed with the quantum simulation are presented in Figure 6 and Table 1, respectively. The quantum effects do not significantly change their average values relative to those of the classical simulation. The O1···O2 distance probability distribution remains almost unaltered. This is expected since these atoms are much heavier than the proton. The probability distribution related to two angles (O1−H−O2 and H−O1−C2) that determine the position of the proton relative to the oxygen atoms become broader with inclusion of the quantum effects. Interestingly, the probability distribution of the dihedral angle that describes out-of-plane motion of the hydroxy group (H−O1−C2-C1) is similar to the classical one.

Infrared Spectrum. It would certainly be desirable to use centroid or ring polymer path integral molecular dynamics[69] in order to properly account the quantum effects[70] necessary for simulation of DBM's infrared spectrum. Nevertheless, we will demonstrate that even classical simulation might qualitatively

DOI: 10.1021/acs.jpca.8b01930
J. Phys. Chem. A 2018, 122, 5945−5954

reproduce the infrared spectrum in this case and provide insight into the vibrational response of the OHO moiety. The origin of this can be understood as follows. In the previous section we showed that nuclear quantum effects mostly modify the in-plane motion of the hydrogen bonded proton in the six-membered ring, whereas other degrees of freedom are not significantly altered. Hence, we could expect that the infrared spectrum simulated by classical molecular dynamics would exhibit certain differences in the ν_{OH} and δ_{OH} modes in comparison to the experimental one. Furthermore, both classical and quantum molecular dynamics predict the small free energy barriers, although with different heights.

The simulated infrared spectra obtained by classical molecular dynamics together with the spectrum computed within harmonic oscillator and linear dipole approximation and the vapor experimental spectrum[71] are shown in Figure 7. Let

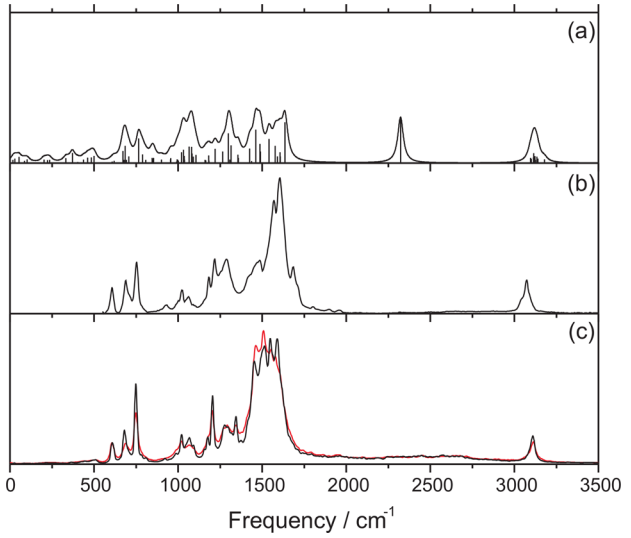

Figure 7. Simulated and experimental infrared spectra: (a) harmonic oscillator spectrum (stick spectrum) and its Lorentzian broadened spectrum with half-width 20 cm^{-1} (solid line), (b) vapor experimental spectrum,[71] and (c) spectra simulated by classical molecular dynamics and averaged over five (red line) and 15 (black line) trajectories.

us first discuss the harmonic oscillator spectrum (see Figure 7a). DBM has 29 atoms and thus 81 vibrational degrees of freedom. The high frequency region of the harmonic oscillator infrared spectrum above 3000 cm^{-1} consists of the 11 C−H stretching modes whose peak maximum is found at 3120 cm^{-1}. The hydrogen-bonded O−H stretching band is found to be at 2323 cm^{-1}. Note that a change in the proton transfer barrier height affects the shape of the potential energy surface in the region around the minima[66] and thus electronic structure methods that provide higher barriers will also give higher harmonic O−H stretching frequencies. Thus, CC2/cc-pVTZ level of theory, which provides only 0.1 kcal/mol higher barrier than the BLYP+D3/GPW method, gives the ν_{OH} harmonic frequency at 2479 cm^{-1}.[54] On the other hand, this frequency amounts to 2938 and 2946 cm^{-1} at the M06-2X/cc-pVTZ and MP2/cc-pVDZ levels of theory,[54] respectively. The O−H stretching intensity in the harmonic approximation is an order of magnitude larger than the C−H intensities. The δ_{OH} and γ_{OH} frequencies equal to 1636 and 1081 cm^{-1}, respectively. The ν_{CO} mode at 1541 cm^{-1} has a lower intensity than the δ_{OH} mode. It is obvious that the harmonic oscillator spectrum fails to describe the two most important characteristics of the experimental spectrum: the very weak intensity of the δ_{OH} mode and the strong intensity of the broad band at around 1600 cm^{-1} (cf. Figure 7a and 7b).

The infrared spectrum simulated by molecular dynamics can be assigned by considering the DBM's and partially deuterated DBM's power spectra of selected degrees of freedom (see Figure 8). The latter species was created by substituting the

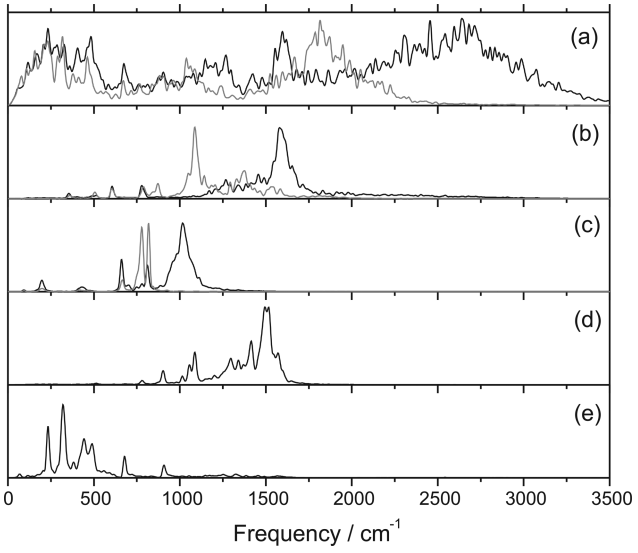

Figure 8. Power spectra of DBM's (black lines) and partially deuterated DBM's (gray lines) selected degrees of freedom: (a) O1−H, (b) H−O1−C2, (c) H−O1−C2−C1, (d) O1−C2, and (e) O1···O2. The atomic labels correspond to the numbering in Figure 2.

hydrogen atom in the OHO moiety with the deuterium atom and its power spectra were computed by averaging over two 20 ps long microcanonical trajectories. The power spectra peak at frequencies at which examined coordinates oscillate. In addition, they contain information about intramolecular couplings and other vibrational properties. Note that classical ab initio molecular dynamics simulations might provide too wide spectral densities of high-frequency modes in comparison to quantum simulations since classical simulations visit a potential energy surface within the high-temperature limit.[72] Also, normal mode softening due to the employed density functional and basis set,[73] shifts vibrational frequencies by several tens of wavenumbers. The O1−H distance power spectrum is given in Figure 8a. It reveals that the hydrogen bond dynamics are active on all frequencies up to 3500 cm^{-1} and that there are extensive couplings to other modes. This power spectrum exhibits a broad band in the spectral range from 2000 to 3500 cm^{-1} with the maximum at approximately 2640 cm^{-1}. The band corresponds to the O−H stretching proton transfer mode. Upon deuteration, its maximum decreases to 1816 cm^{-1}. The strong peak at approximately 1580 cm^{-1} can be attributed to the coupling of the O−H stretching with the in-plane bending motion (see Figure 8b). Deuterating the transferring hydrogen red-shifts this peak to 1085 cm^{-1}. On the other hand, the out-of-plane bending is less coupled to the O−H stretching motion than the in-plane bending. This motion mainly occurs at 1016 and 780 cm^{-1} in DBM and partially deuterated DBM, respectively (see Figure 8c). The in- and out-of-plane bending degrees of freedom were also previously found to be the modes coupled most strongly

DOI: 10.1021/acs.jpca.8b01930
J. Phys. Chem. A 2018, 122, 5945−5954

to the O−H stretching mode.[54] The C−O stretching motion is very weakly coupled to the O−H stretching. Its power spectrum is presented in Figure 8d. The spectrum contains several peaks of which the bands at 1492 and 1517 cm^{-1} have the highest intensities. It is also interesting to examine the O1···O2 distance power spectrum, which is given in Figure 8e. This low-frequency motion has its maximum in the power spectrum at 316 cm^{-1}. It is also considerably coupled to the O−H stretching motion.

With regard to these findings, we proceed to the assignment of the infrared spectrum computed from the molecular dynamics simulation. Our intention in this work is not to obtain a high resolution spectrum, but to qualitatively estimate the positions and intensities of the infrared transitions. We observe a reasonably good agreement between the simulated and experimental spectra. Let us first take a closer look at the intriguing broad band centered around 2700 cm^{-1} in the experimental spectrum. Figure 9 displays the simulated and

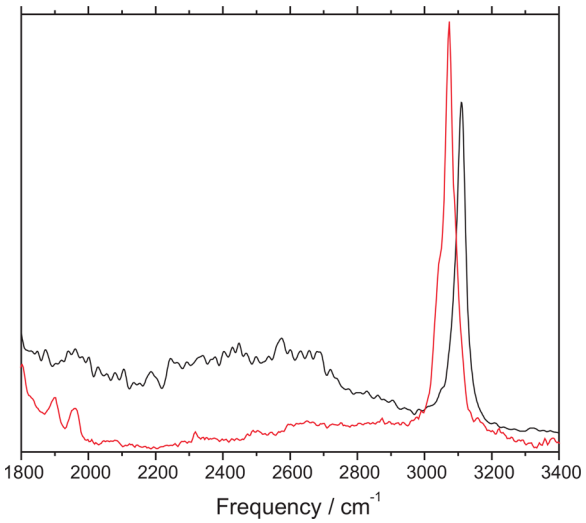

Figure 9. Experimental[71] (red line) and simulated (black line) spectra in the spectral range from 1800 to 3400 cm^{-1}.

experimental spectra in the range from 1800 to 3400 cm^{-1}. On the basis of the O1−H power spectrum, we assign this band to the ν_{OH} motion. The maximum of the simulated band differs from the experimental maximum by approximately 60 cm^{-1}. The maximum of the O−D stretching band in the experimental spectrum of the partially deuterated DBM is found at 1960 cm^{-1} in carbon tetrachloride.[49] By comparing this value to the maximum of the O−D power spectrum, we find a somewhat larger deviation of 140 cm^{-1}. These relatively good agreements provide indirect evidence that the proton transfer barrier has a reasonable value. On the other hand, the simulated intensity is approximately four times larger than the experimental one. This might be due to an uneven energy distribution among individual vibrations during the relatively short time scale of the simulations.[74] In order to examine this possibility, we computed the averaged infrared spectra over five trajectories (see Figure 7c). We do not find significant discrepancy between these spectra in the O−H stretching region, indicating that even five trajectories provide well-stabilized spectral intensities of the O−H stretching band. Thus, the performed molecular dynamics simulations correctly distribute energy into the O−H stretching vibration. A more plausible explanation for the difference between the O−H stretching intensities of the simulated and the experimental spectra could be the limited ability of the BLYP+D3 functional to properly describe the dipole moment surface along the proton degrees of freedom. Furthermore, the classical simulation infrequently samples symmetric O···H···O configurations, which are present in the quantum simulation. These configurations are characterized by a substantial covalent character of the hydrogen bond,[54] which is responsible for a very weak dipole moment change when the proton oscillates. It is also interesting to compare simulated O−H stretching bands of DBM and acetylacetone computed by Meuwly and coworkers.[34] These authors propagated trajectories on the potential energy surface fitted to ab initio calculations at the MP2/6-311++G(d,p) level. Their simulated O−H stretching band intensity exhibits better agreement with the experimental than ours for DBM. This might indicate that a higher level of theory is necessary to obtain better ν_{OH} intensities. We assign the δ_{OH} mode computed at 1580 cm^{-1} to the experimental peak at 1682 cm^{-1} rather than to the peak at 1470 cm^{-1} as Bratož et al.[49] suggested. Similarly, as for the ν_{OH} band, it has an approximately 2.5 times higher intensity than the experimental band. The position of the δ_{OD} mode in the partially deuterated DBM accidentally coincides with the experimental value 1085 cm^{-1} observed in carbon tetrachloride.[49] Intensities of other transitions in the simulated infrared spectrum have good agreement with the experimental ones. The most intense peak in the experimental spectrum comes from the C−O stretching motion. The simulated γ_{OH} peak at 1016 cm^{-1} nicely matches the experimental peak at 1022 cm^{-1}.

CONCLUSIONS

The enolic form of dibenzoylmethane exhibits a strong intermolecular hydrogen bond whose structure and infrared spectrum have been the subject of numerous experimental and theoretical studies.[4,9,10,13,32,42−52,54] Nevertheless, there is no decisive conclusion about the symmetry of its hydrogen bond as well as the position of the ν_{OH} stretching band. In this contribution, we have addressed these issues by using classical and path integral molecular dynamics based on the density functional theory. Our findings indicate that the hydrogen bond is slightly asymmetric with a very small Helmholtz free energy barrier for the proton transfer at room temperature. The proton exchange between the two asymmetric structures proceeds with a time constant, which is approximately equal to 300 fs. The simulated infrared spectrum by classical molecular dynamics is in a resonably good agreement with the vapor experimental spectrum.[71] The simulated ν_{OH} and δ_{OH} bands are located at 2640 and 1580 cm^{-1}, respectively. The discrepancy between intensities of the simulated and experimental ν_{OH} and δ_{OH} transitions is attributed to the employed density functional and quantum effects. We believe that these finding could be of significance for understanding the symmetry and spectral response of short hydrogen bonds in other β-diketone compounds.

AUTHOR INFORMATION

Corresponding Authors

*(M.E.) E-mail: etinski@ffh.bg.ac.rs.
*(B.E.) E-mail: b.ensing@uva.nl.

ORCID

Mihajlo Etinski: 0000-0003-0342-7045

DOI: 10.1021/acs.jpca.8b01930
J. Phys. Chem. A 2018, 122, 5945−5954

Bernd Ensing: 0000-0002-4913-3571

Notes

The authors declare no competing financial interest.

■ ACKNOWLEDGMENTS

M.E. acknowledges the Ministry of Education, Science, and Technological Development of the Republic of Serbia (Contract No. 172040) and the Holland Research School of Molecular Chemistry (HRSMC) for financial support.

■ REFERENCES

(1) Arunan, E.; Desiraju, G. R.; Klein, R. A.; Sadlej, J.; Scheiner, S.; Alkorta, I.; Clary, D. C.; Crabtree, R. H.; Dannenberg, J. J.; Hobza, P.; Kjaergaard, H. G.; Legon, A. C.; Mennucci, B.; Nesbitt, D. J. Defining the Hydrogen Bond: An Account. *Pure Appl. Chem.* **2011**, *83*, 1619−1636.

(2) Benoit, M.; Marx, D. The Shapes of Protons in Hydrogen Bonds Depend on the Bond Length. *ChemPhysChem* **2005**, *6*, 1738−1741.

(3) McKenzie, R. H.; Bekker, C.; Athokpam, B.; Ramesh, S. G. Effect of Quantum Nuclear Motion on Hydrogen Bonding. *J. Chem. Phys.* **2014**, *140*, 174508.

(4) Gilli, P.; Bertolasi, V.; Pretto, L.; Ferretti, V.; Gilli, G. Covalent versus Electrostatic Nature of the Strong Hydrogen Bond: Discrimination among Single, Double, and Asymmetric Single-Well Hydrogen Bonds by Variable-Temperature X-ray Crystallographic Methods in β-Diketone Enol RAHB Systems. *J. Am. Chem. Soc.* **2004**, *126*, 3845−3855.

(5) Baughcum, S.; Duerst, R. W.; Rowe, W. F.; Smith, Z.; Wilson, E. B. Microwave Spectroscopic Study of Malonaldehyde (3-Hydroxy-2-Propenal). 2. Structure, Dipole Moment, and Tunneling. *J. Am. Chem. Soc.* **1981**, *103*, 6296−6303.

(6) Camerman, A.; Mastropaolo, D.; Camerman, N. Molecular Structure of Acetylacetone. A Crystallographic Determination. *J. Am. Chem. Soc.* **1983**, *105*, 1584−1586.

(7) Boese, R.; Antipin, M. Y.; Bläser, D.; Lyssenko, K. A. Molecular Crystal Structure of Acetylacetone at 210 and 110 K: Is the Crystal Disorder Static or Dynamic? *J. Phys. Chem. B* **1998**, *102*, 8654−8660.

(8) Herbstein, F. H.; Iversen, B. B.; Kapon, M.; Larsen, F. K.; Madsen, G. K. H.; Reisner, G. M. X-Ray and Neutron Diffraction Study of Benzoylacetone in the Temperature Range 8−300 K: Comparison with other Cis-Enol Molecules. *Acta Crystallogr., Sect. B: Struct. Sci.* **1999**, *55*, 767−787.

(9) Williams, D. E. Crystal Structure of Dibenzoylmethane. *Acta Crystallogr.* **1966**, *21*, 340−349.

(10) Hollander, F. J.; Templeton, D. H.; Zalkin, A. The Crystal and Molecular Structure of 1,3-Diphenyl-1,3-Propanedione Enol. *Acta Crystallogr., Sect. B: Struct. Crystallogr. Cryst. Chem.* **1973**, *B29*, 1552−1553.

(11) Etter, M. C.; Jahn, D. A.; Urbańczyk-Lipkowska, Z. A New Polymorh of Dibenzoylmethane. *Acta Crystallogr., Sect. C: Cryst. Struct. Commun.* **1987**, *C43*, 260−263.

(12) Kaitner, B.; Mestrović, E. Structure of a New Crystal Modification of 1,3-Diphenyl-1,3-Propanedione. *Acta Crystallogr., Sect. C: Cryst. Struct. Commun.* **1993**, *C49*, 1523−1525.

(13) Thomas, L. H.; Florence, A. J.; Wilson, C. C. Hydrogen Atom Behaviour Imaged in a Short Intramolecular Hydrogen Bond Using the Combined Approach of X-Ray and Neutron Diffraction. *New J. Chem.* **2009**, *33*, 2486−2490.

(14) Tuckerman, M. E.; Marx, D. Heavy-Atom Skeleton Quantization and Proton Tunneling in "Intermediate-Barrier" Hydrogen Bonds. *Phys. Rev. Lett.* **2001**, *86*, 4946−4949.

(15) Tew, D.; Handy, N.; Carter, S.; Irle, S.; Bowman, J. The Internal Coordinate Path Hamiltonian; Application to Methanol and Malonaldehyde. *Mol. Phys.* **2003**, *101*, 3513−3525.

(16) Coutinho-Neto, M. D.; Viel, A.; Manthe, U. The Ground State Tunneling Splitting of Malonaldehyde: Accurate Full Dimensional Quantum Dynamics Calculations. *J. Chem. Phys.* **2004**, *121*, 9207−9210.

(17) Wassermann, T. N.; Luckhaus, D.; Coussan, S.; Suhm, M. A. Proton Tunneling Estimates for Malonaldehyde Vibrations from Supersonic Jet and Matrix Quenching Experiments. *Phys. Chem. Chem. Phys.* **2006**, *8*, 2344−2348.

(18) Viel, A.; Coutinho-Neto, M. D.; Manthe, U. The Ground State Tunneling Splitting and the Zero Point Energy of Malonaldehyde: A Quantum Monte Carlo Determination. *J. Chem. Phys.* **2007**, *126*, 024308.

(19) Wang, Y.; Braams, B. J.; Bowman, J. M.; Carter, S.; Tew, D. P. Full-Dimensional Quantum Calculations of Ground-State Tunneling Splitting of Malonaldehyde Using an Accurate Ab Initio Potential Energy Surface. *J. Chem. Phys.* **2008**, *128*, 224314.

(20) Meyer, R.; Ha, T. Quantum States of Hydrogen Transfer and Vibration in Malonaldehyde. *Mol. Phys.* **2003**, *101*, 3263−3276.

(21) Yang, Y.; Meuwly, M. A Generalized Reactive Force Field for Nonlinear Hydrogen Bonds: Hydrogen Dynamics and Transfer in Malonaldehyde. *J. Chem. Phys.* **2010**, *133*, 064503.

(22) Hammer, T.; Manthe, U. Intramolecular Proton Transfer in Malonaldehyde: Accurate Multilayer Multi-Configurational Time-Dependent Hartree Calculations. *J. Chem. Phys.* **2011**, *134*, 224305.

(23) Schröder, M.; Gatti, F.; Meyer, H. D. Theoretical Studies of the Tunneling Splitting of Malonaldehyde Using the Multiconfiguration Time-Dependent Hartree Approach. *J. Chem. Phys.* **2011**, *134*, 234307.

(24) Wang, Y. M.; Bowman, J. M. Mode-Specific Tunneling Using the Q_{im} Path: Theory and an Application to Full-Dimensional Malonaldehyde. *J. Chem. Phys.* **2013**, *139*, 154303.

(25) Schröder, M.; Meyer, H. D. Calculation of the Vibrational Excited States of Malonaldehyde and Their Tunneling Splittings with the Multi-Configuration Time-Dependent Hartree Method. *J. Chem. Phys.* **2014**, *141*, 034116.

(26) Huang, J.; Buchowiecki, M.; Nagy, T.; Vanicek, J.; Meuwly, M. Kinetic Isotope Effect in Malonaldehyde Determined from Path Integral Monte Carlo Simulations. *Phys. Chem. Chem. Phys.* **2014**, *16*, 204−211.

(27) Dannenberg, J. J.; Rios, R. Theoretical Study of the Enolic Forms of Acetylacetone. How Strong Is the Hydrogen Bond? *J. Phys. Chem.* **1994**, *98*, 6714−6718.

(28) Johnson, M. R.; Jones, N. H.; Geis, A.; Horsewill, A. J.; Trommsdorff, H. P. Structure and Dynamics of the Keto and Enol Forms of Acetylacetone in the Solid State. *J. Chem. Phys.* **2002**, *116*, 5694−5700.

(29) Srinivasan, R.; Feenstra, J. S.; Park, S. T.; Xu, S.; Zewail, A. H. Direct Determination of Hydrogen-Bonded Structures in Resonant and Tautomeric Reactions Using Ultrafast Electron Diffraction. *J. Am. Chem. Soc.* **2004**, *126*, 2266−2267.

(30) Matanović, I.; Došlić, N.; Mihalić, Z. Exploring the Potential Energy Surface for Proton Transfer in Acetylacetone. *Chem. Phys.* **2004**, *306*, 201−207.

(31) Matanović, I.; Došlić, N. Infrared Spectroscopy of the Intramolecular Hydrogen Bond in Acethylacetone: A Computational Approach. *J. Phys. Chem. A* **2005**, *109*, 4185−4194.

(32) Coussan, S.; Ferro, Y.; Trivella, A.; Rajzmann, M.; Roubin, P.; Wieczorek, R.; Manca, C.; Piecuch, P.; Kowalski, K.; Włoch, M.; Kucharski, S. A.; Musiał, M. Experimental and Theoretical UV Characterizations of Acetylacetone and Its Isomers. *J. Phys. Chem. A* **2006**, *110*, 3920−3926.

(33) Belova, N. V.; Oberhammer, H.; Trang, N. H.; Girichev, G. V. Tautomeric Properties and Gas-Phase Structure of Acetylacetone. *J. Org. Chem.* **2014**, *79*, 5412−5419.

(34) Howard, D. L.; Kjaergaard, H. G.; Huang, J.; Meuwly, M. Infrared and Near-Infrared Spectroscopy of Acetylacetone and Hexafluoroacetylacetone. *J. Phys. Chem. A* **2015**, *119*, 7980−7990.

(35) Dolati, F.; Tayyari, S. F.; Vakili, M.; Wang, Y. A. Proton Transfer in Acetylacetone and Its α-Halo Derivatives. *Phys. Chem. Chem. Phys.* **2016**, *18*, 344−350.

DOI: 10.1021/acs.jpca.8b01930
J. Phys. Chem. A 2018, 122, 5945−5954

(36) Lowrey, A. H.; George, C.; D'Antonio, P.; Karle, J. Structure of Acetylacetone by Electron Diffraction. *J. Am. Chem. Soc.* **1971**, *93*, 6399−6403.
(37) Caminati, W.; Grabow, J.-U. The C_{2v} Structure of Enolic Acetylacetone. *J. Am. Chem. Soc.* **2006**, *128*, 854−857.
(38) Feyer, V.; Prince, K. C.; Coreno, M.; Melandri, S.; Maris, A.; Evangelisti, L.; Caminati, W.; Giuliano, B. M.; Kjaergaard, H. G.; Carravetta, V. Quantum Effects for a Proton in a Low-Barrier, Double-Well Potential: Core Level Photoemission Spectroscopy of Acetylacetone. *J. Phys. Chem. Lett.* **2018**, *9*, 521−526.
(39) Verma, P. K.; Steinbacher, A.; Koch, F.; Nuernberger, P.; Brixner, T. Monitoring Ultrafast Intramolecular Proton Transfer Processes in an Unsymmetric β-Diketone. *Phys. Chem. Chem. Phys.* **2015**, *17*, 8459−8466.
(40) Kojić, M.; Petković, M.; Etinski, M. A New Insight into the Photochemistry of Avobenzone in Gas Phase and Acetonitrile from Ab Initio Calculations. *Phys. Chem. Chem. Phys.* **2016**, *18*, 22168−22178.
(41) Kojić, M.; Petković, M.; Etinski, M. Unrevealing Mechanism of the Thermal Tautomerization of Avobenzone by Means of Quantum Chemical Computations. *J. Serb. Chem. Soc.* **2016**, *81*, 1393−1406.
(42) Belova, N. V.; Oberhammer, H.; Girichev, G. V. Tautomeric and Conformational Properties of Dibenzoylmethane, C6H5-C(O)-CH2-C(O)-C6H5: Gas-Phase Electron Diffraction and Quantum Chemical Study. *Struct. Chem.* **2011**, *22*, 269−277.
(43) Jones, R. D. G. The Crystal Structure of the Enol Tautomer of 1,3-Diphenyl-1,3-Propanedione (Dibenzoylmethane) by Neutron Diffraction. *Acta Crystallogr., Sect. B: Struct. Crystallogr. Cryst. Chem.* **1976**, *B32*, 1807−1811.
(44) Borisov, E. V.; Skorodumov, E. V.; Pachevskaya, V. M.; Hansen, P. E. Variable-Temperature NMR Study of the Enol Forms of Benzoylacetones. *Magn. Reson. Chem.* **2005**, *43*, 992−998.
(45) Masuda, Y.; Nakano, T.; Sugiyama, M. First Observation of Ultrafast Intramolecular Proton Transfer Rate between Electronic Ground States in Solution. *J. Phys. Chem. A* **2012**, *116*, 4485−4494.
(46) Mori, Y.; Masuda, Y. Effect of Solvent on Proton Location and Dynamic Behavior in Short Intramolecular Hydrogen Bonds Studied by Molecular Dynamics Simulations and NMR Experiments. *Chem. Phys.* **2015**, *458*, 18−29.
(47) Kong, X.; Brinkmann, A.; Terskikh, V.; Wasylishen, R. E.; Bernard, G. M.; Duan, Z.; Wu, Q.; Wu, G. Proton Probability Distribution in the O···H···O Low-Barrier Hydrogen Bond: A Combined Solid-State NMR and Quantum Chemical Computational Study of Dibenzoylmethane and Curcumin. *J. Phys. Chem. B* **2016**, *120*, 11692−11704.
(48) Rasmussen, R. S.; Tunnicliff, D. D.; Brattain, R. R. Infrared and Ultraviolet Spectroscopic Studies on Ketones. *J. Am. Chem. Soc.* **1949**, *71*, 1068−1072.
(49) Bratož, S.; Hadži, D.; Rossmy, G. The Infra-Red Absorption Bands Associated with the Chelate Ring in Some Unsaturated Hydroxicarbonyl Compounds. *Trans. Faraday Soc.* **1956**, *52*, 464−470.
(50) Tayyari, S. F.; Zeegers-Huyskens, T.; Wood, J. L. Spectroscopic Study of Hydrogen Bonding in the Enol Form of β-Diketones - I. Vibrational Assignment and Strength of the Bond. *Spectrochim. Acta, Part A* **1979**, *35*, 1265−1276.
(51) Tayyari, S. F.; Zeegers-Huyskens, T.; Wood, J. L. Spectroscopic Study of Hydrogen Bonding in the Enol Form of β-Diketones − II. Symmetry of the Hydrogen Bond. *Spectrochim. Acta, Part A* **1979**, *35*, 1289−1295.
(52) Hansen, B. K.; Winther, M.; Spanget-Larsen, J. Intramolecular Hydrogen Bonding. Spectroscopic and Theoretical Studies of Vibrational Transitions in Dibenzoylmethane Enol. *J. Mol. Struct.* **2006**, *790*, 74−79.
(53) Athokpam, B.; Ramesh, S. G.; McKenzie, R. H. Effect of Hydrogen Bonding on the Infrared Absorption Intensity of OH Stretch Vibrations. *Chem. Phys.* **2017**, *488*−*489*, 43−54.
(54) Petković, M.; Etinski, M. Intramolecular OHO bonding in Dibenzoylmethane: Symmetry and Spectral Manifestations. *RSC Adv.* **2014**, *4*, 38517−38526.
(55) VandeVondele, J.; Krack, M.; Mohamed, F.; Parrinello, M.; Chassaing, T.; Hutter, J. QUICKSTEP: Fast and Accurate Density Functional Calculations using a Mixed Gaussian and Plane Waves Approach. *Comput. Phys. Commun.* **2005**, *167*, 103−128.
(56) Becke, A. D. Density-Functional Exchange-Energy Approximation with Correct Asymptotic-Behavior. *Phys. Rev. A: At., Mol., Opt. Phys.* **1988**, *38*, 3098−3100.
(57) Lee, C. T.; Yang, W. T.; Parr, R. G. Development of the Colle-Salvetti Correlation-Energy Formula into a Functional of the Electron-density. *Phys. Rev. B: Condens. Matter Mater. Phys.* **1988**, *37*, 785−789.
(58) Grimme, S.; Antony, J.; Ehrlich, S.; Krieg, H. A Consistent and Accurate Ab Initio Parametrization of Density Functional Dispersion Correction (DFT-D) for the 94 Elements H-Pu. *J. Chem. Phys.* **2010**, *132*, 154104.
(59) Lippert, G.; Hutter, J.; Parrinello, M. A Hybrid Gaussian and Plane Wave Density Functional Scheme. *Mol. Phys.* **1997**, *92*, 477−487.
(60) Goedecker, S.; Teter, M.; Hutter, J. Separable Dual-Space Gaussian Pseudopotentials. *Phys. Rev. B: Condens. Matter Mater. Phys.* **1996**, *54*, 1703−1710.
(61) Genovese, L.; Deutsch, T.; Neelov, A.; Goedecker, S.; Beylkin, G. Efficient Solution of Poisson's Equation with Free Boundary Conditions. *J. Chem. Phys.* **2006**, *125*, 074105.
(62) Genovese, L.; Deutsch, T.; Goedecker, S. Efficient and Accurate Three-Dimensional Poisson Solver for Surface Problems. *J. Chem. Phys.* **2007**, *127*, 054704.
(63) Bussi, G.; Donadio, D.; Parrinello, M. Canonical Sampling Through Velocity Rescaling. *J. Chem. Phys.* **2007**, *126*, 014101.
(64) Brehm, M.; Kirchner, B. TRAVIS - A Free Analyzer and Visualizer for Monte Carlo and Molecular Dynamics Trajectories. *J. Chem. Inf. Model.* **2011**, *51*, 2007−2023.
(65) Thomas, M.; Brehm, M.; Fligg, R.; Voehringer, P.; Kirchner, B. Computing Vibrational Spectra from Ab Initio Molecular Dynamics. *Phys. Chem. Chem. Phys.* **2013**, *15*, 6608−6622.
(66) Mackeprang, K.; Xu, Z.-H.; Maroun, Z.; Meuwly, M.; Kjaergaard, H. G. Spectroscopy and Dynamics of Double Proton Transfer in Formic Acid Dimer. *Phys. Chem. Chem. Phys.* **2016**, *18*, 24654−24662.
(67) Marston, C. C.; Balint-Kurti, G. G. The Fourier Grid Hamiltonian Method for Bound State Eigenvalues and Eigenfunctions. *J. Chem. Phys.* **1989**, *91*, 3571−3576.
(68) Belot, J. A.; Clark, J.; Cowan, J. A.; Harbison, G. S.; Kolesnikov, A. I.; Kye, Y.-S.; Schultz, A. J.; Silvernail, C.; Zhao, X. The Shortest Symmetrical O-H···O Hydrogen Bond Has a Low-Barrier Double-Well Potential. *J. Phys. Chem. B* **2004**, *108*, 6922−6926.
(69) Witt, A.; Ivanov, S. D.; Shiga, M.; Forbert, H.; Marx, D. On the applicability of centroid and ring polymer path integral molecular dynamics for vibrational spectroscopy. *J. Chem. Phys.* **2009**, *130*, 194510−194510−15.
(70) Ramírez, R.; López-Ciudad, T.; Kumar P, P.; Marx, D. Quantum Corrections to Classical Time-Correlation Functions: Hydrogen Bonding and Anharmonic Floppy Modes. *J. Chem. Phys.* **2004**, *121*, 3973.
(71) Infrared Spectra. In *NIST Chemistry WebBook, NIST Standard Reference Database Number 69*; Linstrom, P. J., Mallard, W. G.; Eds., National Institute of Standards and Technology: Gaithersburg MD, http://webbook.nist.gov (retrieved April 3, 2014).
(72) Hudecová, J.; Hopmann, K. H.; Bouř, P. Correction of Vibrational Broadening in Molecular Dynamics Clusters with the Normal Mode Optimization Method. *J. Phys. Chem. B* **2012**, *116*, 336−342.
(73) Milovanović, B.; Kojić, M.; Petković, M.; Etinski, M. New Insight into Uracil Stacking in Water from ab Initio Molecular Dynamics. *J. Chem. Theory Comput.* **2018**, *14*, 2621.

DOI: 10.1021/acs.jpca.8b01930
J. Phys. Chem. A 2018, 122, 5945−5954

(74) Horníček, J.; Kaprálová, P.; Bouř, P. Simulations of Vibrational Spectra from Classical Trajectories: Calibration with ab Initio Force Fields. *J. Chem. Phys.* **2007**, *127*, 084502.

DOI: 10.1021/acs.jpca.8b01930
J. Phys. Chem. A 2018, 122, 5945−5954